Crystal Structure of a Fluorescent Derivative of RNase A‡

Sylvie Baudet-Nessler, Magali Jullien,§ Marie-Pierre Crosio, and Joël Janin*

Laboratoire de Biologie Structurale, UMR 9920 CNRS-Université Paris-Sud, Bât. 433, 91405-Orsay, France

Received January 12, 1993; Revised Manuscript Received March 29, 1993

ABSTRACT: The crystal structure of RNase A chemically modified with the fluorescent probe, *N*-[[(iodoacetyl)-amino]ethyl]-5-naphthylamine-1-sulfonic acid (1,5-IAENS), has been solved and refined to high resolution. It yields information on the mode of binding, the mobility of a probe commonly used in spectroscopic studies, and anion binding sites in RNase A. Trigonal crystals of the fluorescent derivative grown in sodium or cesium chloride and ammonium sulfate, pH 5.1, were nearly isomorphous with those of a semisynthetic RNase [DeMel, et al. (1992) *J. Biol. Chem. 267*, 247–256]. Refinement starting from semisynthetic RNase led to a model with $R = 20\%$ against 1.7-Å diffraction data from crystals in ammonium sulfate and another model with $R = 17\%$ against 1.9-Å data taken in the presence of 3 M NaCl. The second model contains three chloride ions: one is at the active site, and the other two are at molecular interfaces. Otherwise, the two models are very similar. The fluorophore has very little effect on the protein conformation. It is found to be covalently attached to the active site His-12 with the naphthyl group stacked on the imidazole ring of His-119. It remains largely accessible to solvent and in a polar environment on the protein surface, even though the fluorescence emission spectrum is blue shifted as it is in nonpolar solvents.

We report here two X-ray structures of a modified form of bovine pancreatic ribonuclease A (RNase A) obtained by reaction with *N*-[[(iodoacetyl)amino]ethyl]-5-naphthylamine-1-sulfonic acid (1,5-IAENS), which alkylates a catalytic histidine. These structures are of particular interest as the fluorescence anisotropy of the labeled protein has been used to study the early steps of RNase A crystallization (Jullien & Crosio, 1991).

The two histidine residues at the active site of RNase A easily react with halo acids or amides to yield an inactive enzyme. The product of reaction with 1,5-IAENS is AENS-RNase. The AENS label is a convenient probe of protein conformation. In the native protein, spectroscopic characteristics of the bound fluorophore suggest that it has a nonpolar environment at the active site. The polarization or anisotropy of the fluorescence under polarized light excitation is sensitive to the rotational motion of the whole protein (Jullien & Garel, 1981). Self-association slows the rotation and increases anisotropy, and this can be followed in crystallization studies. As the magnitude of this effect depends on the orientation and mobility of the probe, it was important (i) to check that the labeled protein has a similar structure to native RNase A, (ii) to check that the AENS is buried in the active site, and (iii) to determine its position and orientation. This could best be done in a crystallographic study of the labeled protein.

Structures of AENS-RNase were obtained from trigonal crystals in the presence or absence of NaCl and refined to low *R* factors against high-resolution X-ray data. They closely resemble an RNase analog in which a synthetic peptide (111–124) associates with the 1–118 proteolytic fragment (Martin et al., 1987). The crystals of the semisynthetic protein were nearly isomorphous to ours, and we could use it as a starting model for refinement. The main difference between the two AENS-RNase models is the presence of three bound chloride ions in the NaCl structure. The fluorophore is covalently attached to $N^{\epsilon 2}$ of His-12. The (acetylamino)ethyl linker group is involved in polar interactions and is buried in the protein. The naphthyl group is stacked on the imidazole ring of His-119, with one face accessible to solvent. These results are compatible with fluorescence data, which are discussed in view of the three-dimensional structure.

MATERIALS AND METHODS

Preparation of AENS-RNase. RNase A (type XII-A) and 1,5-IAENS were from Sigma. The protein was alkylated with 1,5-IAENS as previously described (Jullien & Garel, 1981). While both catalytic His-12 and His-119 can react, alkylation of one of the two histidines blocks the reaction with the other (Heinrikson et al., 1965). The alkylated protein was purified by ion exchange chromatography, which yields a major peak with 1:1 labeling stoichiometry and no activity (Jullien & Garel, 1981). Cyanogen bromide cleavage after Met-13 releases a fluorescent N-terminal peptide, showing that the AENS group is attached to His-12 (M. Jullien, unpublished data).

Crystallization. Crystals of AENS-RNase were obtained by vapor diffusion in hanging drops under the same conditions as those used for semisynthetic ribonuclease (Doscher et al., 1983), i.e., 3 M CsCl and 20% ammonium sulfate in 50 mM acetate buffer (pH 5.1) at 20 °C. Protein homogeneity in the crystals was checked by FPLC chromatography on Mono-S. The same procedure yields isomorphous crystals with native RNase A, indicating that the modification does not affect crystallization. We also obtained isomorphous crystals by replacing CsCl with NaCl in the crystallization mixture (Crosio & Jullien, 1992). Diffraction data were collected on AENS-RNase crystals grown under both conditions. Those with NaCl were mounted directly from the hanging drop into the capillary. Those with CsCl were soaked into 80% ammonium sulfate before mounting lest X-ray absorption by cesium interfere with data collection. Both types of crystals diffracted to high resolution. They belong to space group $P3_221$ with one molecule per asymmetric unit, and the cell parameters are very similar to those reported for variants of the semisynthetic RNase by DeMel et al. (1992). Their characteristics are summarized in Table I.

‡ Data from this study have been deposited in the Protein Data Bank under file names 1RAR and 1RAS.

* Corresponding author.

§ Present address: CRBM, Route de Mende, 34033-Montpellier, France.

0006-2960/93/0432-8457$04.00/0

Table I: Characteristics of AENS-RNase Crystals

	AENS-RNase		
	type I	type II	semisynthetic RNase[a]
ammonium sulfate	80%	20%	80%
salt	[b]	3 M NaCl	[b]
space group	$P3_221$	$P3_221$	$P3_221$
cell parameters (Å)			
$a = b$	65.1	65.0	64.7
c	65.0	65.0	64.9

[a] D121A variant of semisynthetic RNase (DeMel et al., 1992). [b] Crystals grown in 3 M CsCl were soaked in 80% ammonium sulfate.

X-ray Data Collection and Processing. X-ray diffraction data were collected on station W32 of the LURE (Orsay, France) wiggler line. The wavelength was set to 0.91 Å and the crystals were kept at 5 °C during data collection. Discrete frames of 1.5° oscillation were recorded on an image plate system with exposure times of 1.5–2 min. Two complete data sets were obtained, one from each crystal. After spot integration with the XENGEN program system (Howards et al., 1987), data were processed with the Program Suit for Protein Crystallography distributed by CCP4 (Daresbury, England). A statistical summary of the crystallographic data is presented in Table II. The quality of data was generally better in data set II, and this is also apparent in the statistics on the refined model (see below).

The Starting Model. Structure factors were calculated in the AENS-RNase unit cell with atomic coordinates of the D121A variant of a semisynthetic RNase described in file 4SRN of the Protein Data Bank (Bernstein et al., 1977). They had an R factor of 40% against AENS-RNase data between 10- and 2.5-Å resolution. Rigid body refinement with CORELS (Sussmann et al., 1977) rotated the model by 1.9° and brought the R factor down to 37.5%. As the semisynthetic molecule is in two fragments missing a bond between residues 113 and 114, other high-resolution RNase A structures were also tested as starting models. Monoclinic RNase A, refined to 1.26 Å by Wlodawer et al. (1988), and two derivatives with nucleoside analogs covalently bound to His-12 and His-119 (Nachman et al., 1990) were of special interest in our case. However, all gave initial R factors larger than 42% against our data after superposition onto the 4SRN model, so that the semisynthetic RNase structure was retained.

A model of the AENS molecule was built by M.-C. Vaney (Laboratoire de Minéralogie-Cristallographie, Université Paris 6, Paris, France) using the program SYBYL from Tripos Associates.

Crystallographic Refinement. Least-squares refinement with PROLSQ (Hendrickson, 1985) proceeded in parallel against both data sets. The version we used included fast Fourier structure factor calculation (Finzel, 1987) and could handle intermolecular contacts and multiple side chain conformations (Sheriff, 1987). $3F_{obs} - 2F_{calc}$ and $F_{obs} - F_{calc}$ maps were examined with FRODO (Jones, 1978) on an Evans & Sutherland PS390 graphics system.

After a few cycles of refinement, modified residues 113, 114, and 121 of the 4SRN model were fit to the map. Other residues, including His-119 at the active site, were also adjusted. The N-terminal Lys-1 could not be located and is missing from the models. Peaks larger than 3σ in $F_{obs} - F_{calc}$ maps were interpreted as solvent if they were within hydrogen-bonding distance of protein atoms. The AENS molecule was included in the model as interpretable density appeared next to His-12 in the active site. The bond between His-12 $N^{\epsilon 2}$ and AENS C'_1 was restrained to 1.45 Å. A few side chains clearly had multiple conformations in both models. Their relative occupancies were estimated from the appearance of electron density and adjusted to give similar temperature factors after refinement.

Table II: AENS-RNase Data Collection and Structure Refinement

		model I (no NaCl)	model II (3 M NaCl)
Data Collection			
resolution (Å)		1.7	1.9
rotation range (deg)		63	45
reflections			
total		53253	33373
unique		19015	11273
merging R factor[a]		7.4%	5.5%
completeness		89%	88%
outer resolution shell[b]		99%	98%
Refinement			
resolution range (Å)		6.0–1.7	6.0–1.9
R factor (%)		20.3	17.2
reflections used[c]		14206	10540
mean B factor (Å^2)		23.0	18.5
atoms			
total		1063	1072
protein		942	944
AENS		21	21
water		100	104
chloride			3
Stereochemistry[d]			
distances (Å)			
bond lengths	0.02	0.013	0.012
angles 1–3	0.04	0.040	0.037
planar 1–4	0.04	0.038	0.035
planes	0.02	0.011	0.010
chiral volumes (Å^3)	0.05	0.032	0.030
nonbonded (Å)			
single torsion	0.5	0.182	0.172
multiple torsion	0.5	0.302	0.254
H-bond	0.5	0.234	0.261
intermolecular (Å)			
multiple torsion	0.5	0.410	0.285
H-bond	0.5	0.400	0.257
torsion angles (deg)			
planar	3	2.02	1.93
staggered	10	17.0	13.9
orthonormal	15	22.1	20.4
B factors (Å^2)			
main chain 1–2	1.0	0.83	0.81
1–3	1.0	1.45	1.40
side chain 1–2	1.0	1.17	1.08
1–3	1.5	1.94	1.46

[a] R merge = $\sum|I_{hkl} - \bar{I}_{hkl}|/\sum I_{hkl}$. [b] From 1.84- to 1.71-Å resolution for data set I and from 2.08- to 1.92-Å resolution for data set II. [c] F larger than $3\sigma_F$. [d] Values in column 2 are input standard deviations and in columns 3 and 4 rms deviations from reference values.

Final cycles of refinement used all data with $F_{obs} > 3\sigma_F$. The R factor of model I (no NaCl) was 20% at 1.7-Å resolution, and that of model II (3 M NaCl) was 17% at 1.9 Å. The dependence with resolution (Figure 1) is compatible with an rms error in atomic positions of 0.25 Å. The quality of the stereochemistry in the refined structures can be judged from a summary of refinement statistics (Table II). In both models, all non-glycine residues except Gln-60, which is located in a sharp turn and has the same unusual conformation in native RNase (Wlodawer et al., 1982), were within the permitted area of the Ramachandran plot.

RESULTS

RNase Structure. The RNase molecule is essentially the same in a large number of crystal forms studied to high resolution (Wlodawer, 1985). This is true for models I and II of the AENS derivative. They differ by only 0.19 Å rms

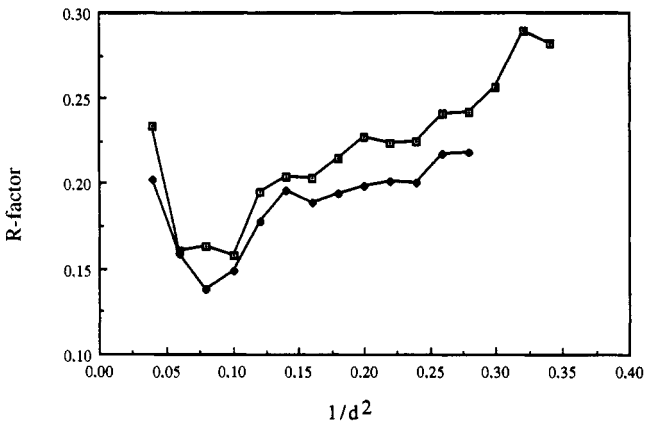

FIGURE 1: Crystallographic *R* factor *vs* resolution: (□) model I, 1.7-Å data taken in 80% ammonium sulfate; (●) model II, 1.9-Å data taken in 20% ammonium sulfate and 3 M NaCl.

on C^{α} atoms and 0.66 Å for all common atoms, including AENS and 65 solvent molecules. No main chain atom position differs by more than 0.4 Å and no side chain atom differs by more than 1 Å, except in a few regions with high temperature factors. The two protein models are therefore identical within experimental error; the AENS moieties and most of the solvent structures are also. Poor electron density was observed for N-terminal Lys-1 and also for Ser-21, which is at the cleavage site in RNase S. In crystal packing, the Lys-1 from one AENS-RNase molecule is close to the Ser-21 of another. Residues 14–23, 35–40, 66–70, 87–94, and 111–117 have higher than average temperature factors. These residues are in external loops of the polypeptide chain. The most disordered region is segment 87–94, as in the orthorhombic cross-linked RNase structure reported by Wlodawer et al. (1988), who mention that it may be involved in early steps of unfolding.

A ribbon tracing of the polypeptide chain with the fluorophore attached is shown in Figure 2. The rms discrepancy from monoclinic RNase A is 0.44 Å for all C^{α} atoms, which is larger than the estimated error but comparable to differences observed between other well-refined X-ray structures of the same protein in different crystal forms (Chothia & Lesk, 1986). Only segments with high *B* factors mentioned above show discrepancies larger than 0.5 Å. The overall correlation with our starting model, trigonal semisynthetic RNase variant D121A, is slightly worse: 0.55 Å for all C^{α}. However, the large discrepancy at residues 112–113 (Figure 3) is an artifact of the discontinuity in semisynthetic RNase, while main chain movements larger than 1 Å in loop 64–70 may be related to the amino acid substitution in the D121A variant. It removes a hydrogen bond between the NH of Lys-66 and the carboxylate of Asp-121 (DeMel et al., 1992). In other regions of the polypeptide chain, the rms C^{α} distance is only 0.34 Å, on the order of the estimated error. Thus, the bound fluorophore has little effect on main chain conformation.

Active Site. At the active site, His-12 has its side chain in the *gauche*$^{+}$ conformation, as in other RNase structures (Martin et al., 1987), in spite of the covalent bond with AENS. The χ_1 angle is $-60 \pm 3°$ in models I and II. It is $-55°$ in monoclinic RNase A (file 7RSA). The $N^{\delta 1}$ atom hydrogen bonds to the carbonyl group of Thr-45 and the $N^{\epsilon 2}$ atom to the acetyl group of AENS, which implies that both nitrogens are protonated at pH 5.1. The other active site histidine is His-119, for which two conformations have been described in different crystal structures. In AENS-RNase, only one is found: His-119 is *trans* with $\chi_1 = 180°$ in both models and a possible hydrogen bond from $N^{\epsilon 2}$ to the carbonyl of Phe-120. This corresponds to position A of the imidazole group as reported by Borkakoti et al. (1982). The starting model had His-119 in position B (*gauche*$^{+}$, $\chi_1 = -50°$).

Two side chains in the vicinity of the active site, those of Asp-121 and Lys-66, differ in models I and II. In model II, the electron density was unambiguous for both. The Asp-121 side chain is *trans* ($\chi_1 = -167°$); the carboxylate interacts with the NH of Lys-66 as noted by DeMel et al. (1992) and also with the guanidinium group of Arg-85 from a neighboring molecule in the crystal. In model I, the density indicated disorder for Lys-66 and a preference for the *gauche*$^{+}$ conformation ($\chi_1 = -63°$) for Asp-121, with the carboxylate pointing toward the 65–72 disulfide bridge. The short distance to the Cys-72 S^{γ} is compatible with a protonated Asp-121 hydrogen bonding to the sulfur. These changes are not obviously related to the solvent composition, and it is likely that the two conformations are in equilibrium.

The Fluorophore. Unlike the protein component, most of the AENS substituent remained poorly defined in the electron

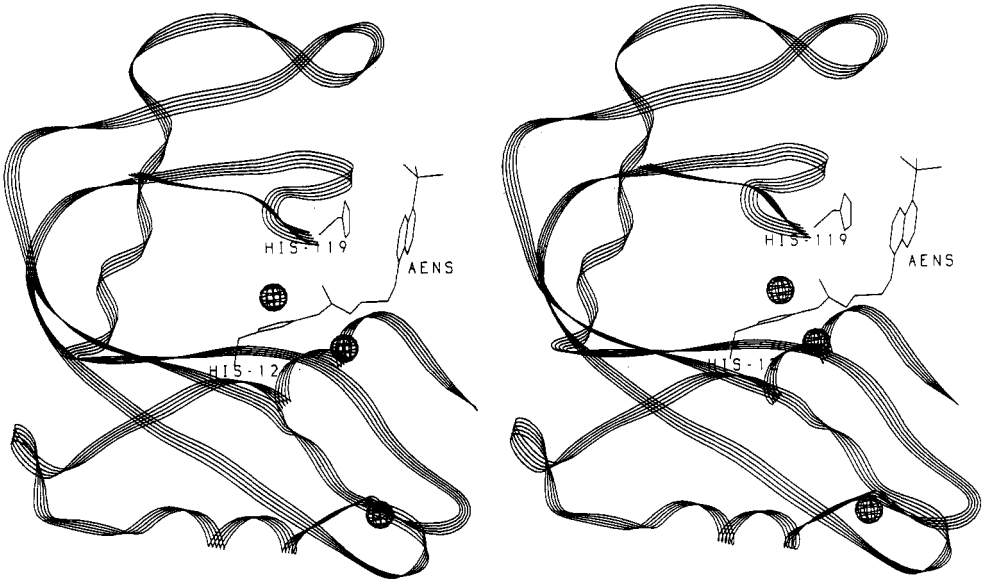

FIGURE 2: Overview of AENS-RNase. The two catalytic histidines, the fluorophore attached to His-12, and the three chloride ions identified in model II are detailed.

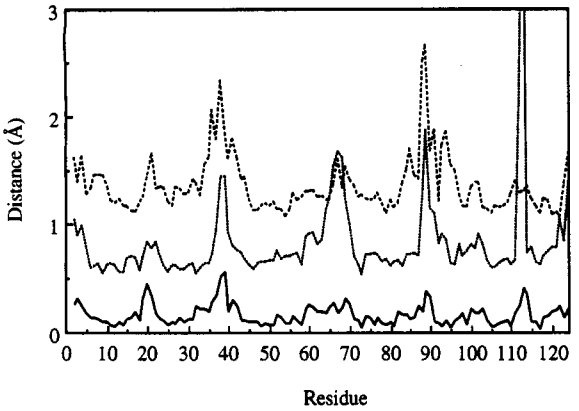

FIGURE 3: Distances between C^{α} atoms after least-squares superposition: (—) models I and II of AENS-RNase (rms = 0.19 Å); (- - -) model I of AENS-RNase and monoclinic RNase A (Wlodawer et al., 1988) (the curve is shifted upward by 1 Å; rms = 0.5 Å); (···) model I of AENS-RNase and trigonal semisynthetic RNase variant D121A, the starting model for refinement of AENS-RNase, which has a break at residue 113 and a substitution at Asp-121 (De Mel et al., 1992) (the curve is shifted upward by 0.5 Å; rms = 0.55 Å).

density map until late in the refinement. At early stages, only the (acetylamino)ethyl linker group could be unambiguously located in $3F_{obs} - 2F_{calc}$ maps as density extending from the His-12 imidazole; the naphthyl and sulfonate moieties had no observable density. Nevertheless, the most prominent features of $F_{obs} - F_{calc}$ omit maps were density adjacent to His-119, in which the electron-rich sulfonate group and part of the naphthyl ring could be located (Figure 4). After refinement, the $3F_{obs} - 2F_{calc}$ density was still weak, and the ring *B* factors were higher than those for the linker group (Table III) or the His-119 imidazole. This indicates disorder, but no alternative position of the naphthyl ring is compatible with the density and the stereochemistry of the linker group. Thus, the final models have all atoms of the fluorescent probe in this position with full occupancy.

The (acetylamino)ethyl linker is covalently attached to $N^{\epsilon 2}$ of His-12 through the C'_1 atom. In addition, it makes two hydrogen bonds to the protein: the acetyl group hydrogen bonds to the main chain NH of Phe-120, and the amino N'_3 bonds to the side chain amide group of Gln-11. The distal ring of the naphthyl chromophore is stacked on the imidazole

Table III: Temperature Factors and Solvent-Accessible Area of the AENS Fluorophore

group	av B^a (Å^2)	solvent-accessible area^b (Å^2) bound	free
(acetylamino)ethyl linker	21.7	32	201
naphthyl ring			
proximal ring	32.1	76	99
distal ring	30.1	44	84
sulfonate	34.1	66	111
total	28.9	218	495

^{a} Average of atomic *B* factors in model I. The linker group has seven atoms, each of the two rings has five, and the sulfonate has four. ^{b} Accessible surface areas were calculated on model I using program ASA from Prof. A. Lesk (Cambridge) and a probe size of 1.4 Å.

of His-119, with the two planes 3.5 Å apart. The proximal ring is not in contact with the protein. The sulfonate group on the distal ring is surrounded by the side chains of Asn-67, Gln-69, and Asn-71, yet it appears to make only one direct interaction with the amide group of Asn-67 (Figure 5). Consequently, the naphthyl and sulfonate groups remain largely accessible to solvent, while the linker group is mostly buried inside the protein (Table III).

Chloride Binding. The most significant difference observed between the two refined structures of AENS-RNase concern solvent regions. Model I was derived from crystals grown in CsCl and soaked in ammonium sulfate for an hour before mounting. CsCl was effectively washed out, and no electron density in the solvent region could be attributed to bound Cs^+ or Cl^- ions. In other RNase A crystal structures done in the presence of phosphate or sulfate (Wlodawer et al., 1982, 1988; Campbell & Petsko, 1987), including trigonal semisynthetic RNase, an anion is found at the active site. In our case, the anion site overlaps with the fluorophore and no bound sulfate was observed.

Model II was obtained in the presence of 3 M NaCl. All peaks larger than 3.5σ in $F_{obs} - F_{calc}$ maps were carefully examined for density attributable to bound Na^+ or Cl^-. The anion has 18 electrons and should be easily distinguished from water molecules. The cation has only 10, and we had to rely on its coordination. Three chloride ions, but no sodium, were located in model II (Figure 6). They have high electronic density and *B* factors less than 24 Å^2 when refined with full occupancy. Chloride 1 is in the active site region near His-12

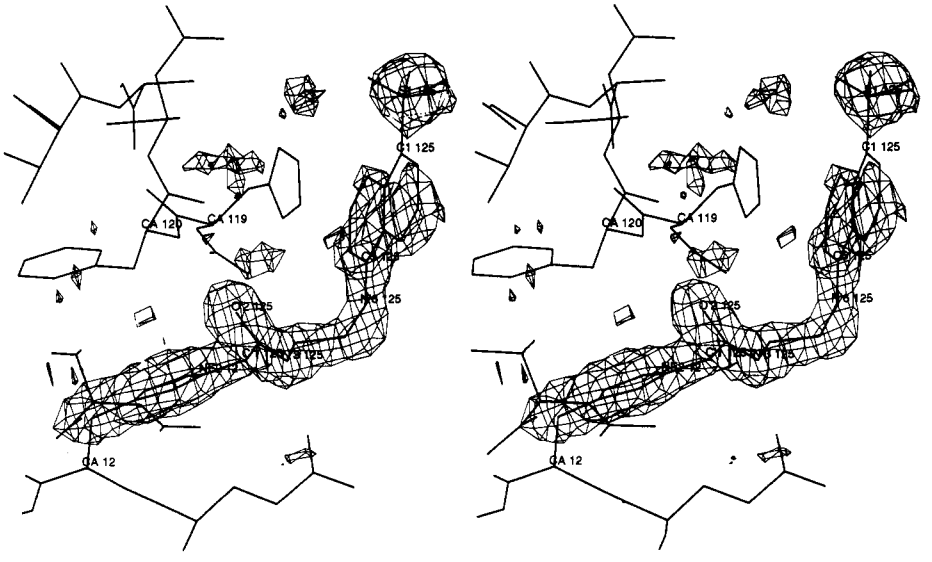

FIGURE 4: Electron density map of the AENS fluorophore. $F_{obs} - F_{calc}$ map calculated after omission of the His-12 side chain and AENS atoms in model II, contoured at 1.5σ.

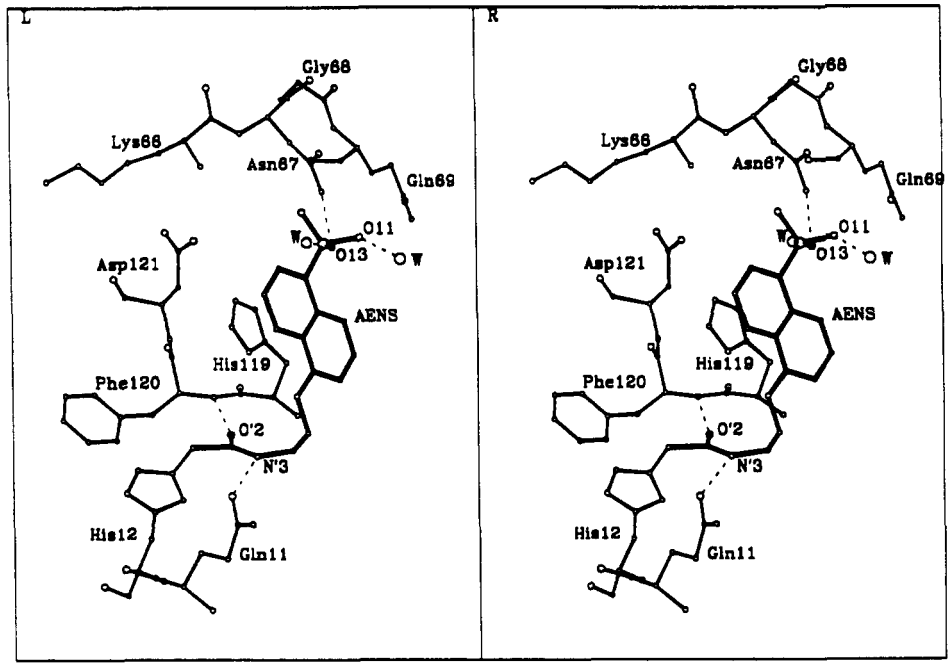

FIGURE 5: Interactions of the AENS fluorophore at the RNase active site. The fluorophore (full bonds) is covalently attached to His-12 and stacked on His-119. Possible hydrogen bonds are indicated.

and possibly interacts with $N^{\delta 1}$, but not at the sulfate binding site. The anion is within 3.6 Å of the main chain NH and side chain OH of Thr-45 and less than 3 Å from a water molecule. Except for His-12, which is probably protonated at pH 5.1, the nearest positive charge is on the Lys-41 almost 5 Å away.

Chlorides 2 and 3 are at interfaces between RNase molecules in the crystal packing. Chloride 2 is within 4 Å of the Arg-10 guanidinium group and the Asn-34 amide from one RNase molecule and the Thr-77 and Ser-78 hydroxyls from another molecule. In addition, chloride 2 is 3 Å from a water molecule that bridges Glu-2 and His-105 through the molecular interface. Chloride 3 has fewer interactions with protein atoms: it is in direct contact only with the Thr-3 hydroxyl. However, a well-defined network of water molecules also links it to several charged groups on two neighboring RNase molecules; the nearest one is the Lys-98 ϵ-amino.

In model I, water molecules replace the three chloride ions. They form the same bonds with the protein atoms, which move by less than 0.5 Å. Otherwise, the solvent structure is the same as in model II, with 62 of the 103 water molecules being less than 1 Å apart. Wlodawer et al. (1988) mention a water molecule buried in a shallow pocket of monoclinic RNase A close to a 2-methyl-2-propanol binding site. The water molecule is also present here; it hydrogen bonds to the carbonyls of Ser-23 and Tyr-97 and to the Thr-99 hydroxyl.

Crystal Packing and Intermolecular Interactions. Like all crystal forms of RNase obtained in high salt, the trigonal form studied here contains an RNase dimer. In space group $P3_221$, its 2-fold axis is crystallographic, while it is a local 2-fold in space groups of lower symmetry. The dimer has the same large interface in both situations. Dimerization may be the first step in RNAse crystallization under high salt conditions (Crosio et al., 1992; Svensson et al., 1991). The two active sites in the AENS-RNase dimer face each other, yet they are far apart. The naphthyl rings are almost orthogonal to the 2-fold axis and parallel to each other, but they are 15 Å apart and the fluorophore plays no part in dimer formation or in crystal packing.

DISCUSSION

Fluorescence spectroscopy is a powerful tool to study protein dynamics. It makes use of intrinsic chromophores, mostly tryptophan residues, or extrinsic reporter groups. When fluorescent aromatic dyes adsorb on proteins, changes in spectroscopic properties yield information on their physical–chemical environment in the protein. Hydrophobic probes such as naphthylaminesulfonate have a much higher quantum yield in nonpolar solvents than in water. Their fluorescence is also enhanced when they bind to proteins, providing a sensitive spectroscopic signal for binding (Stryer, 1968). Moreover, the lifetime of the excited state is long, comparable to the rotational relaxation time of medium-sized proteins. Thus, the fluorescence anisotropy can be used to determine the relaxation time.

The iodoacetamide group of 1,5-IAENS was designed to covalently attach a fluorescent naphthylaminesulfonate probe onto sulfhydryl groups. In their absence, it can also alkylate histidines. The AENS derivative has an excitation maximum near 340 nm; as in other naphthylamines, it involves at least two electronic transitions yielding overlapping bands (Hudson & Weber, 1973). The emission maximum shifts continuously from 520 nm in water down to 450 nm in nonpolar solvents, while the quantum yield and fluorescence lifetime increase. The difference between excitation and emission wavelengths is the Stokes shift, which is attributed to solvent effects and is sensitive to solvent polarity. In the excited state, chromophore molecules usually have a larger electric dipole than in the ground state. The solvent molecules reorient around them, and some of the interaction energy is lost when the chromophore returns to the ground state.

AENS has been used as a conformational probe for RNase A (Jullien et al., 1981, 1986). AENS-RNase has an emission maximum near 480 nm and a fluorescence decay time of 20 ns in the native state. The maximum moves to 500 nm upon unfolding by guanidinium chloride, while the quantum yield and decay time decrease by one-half. The fluorescence anisotropy is large in the native state. Its decay time is compatible with a rigidly fixed AENS group rotating with

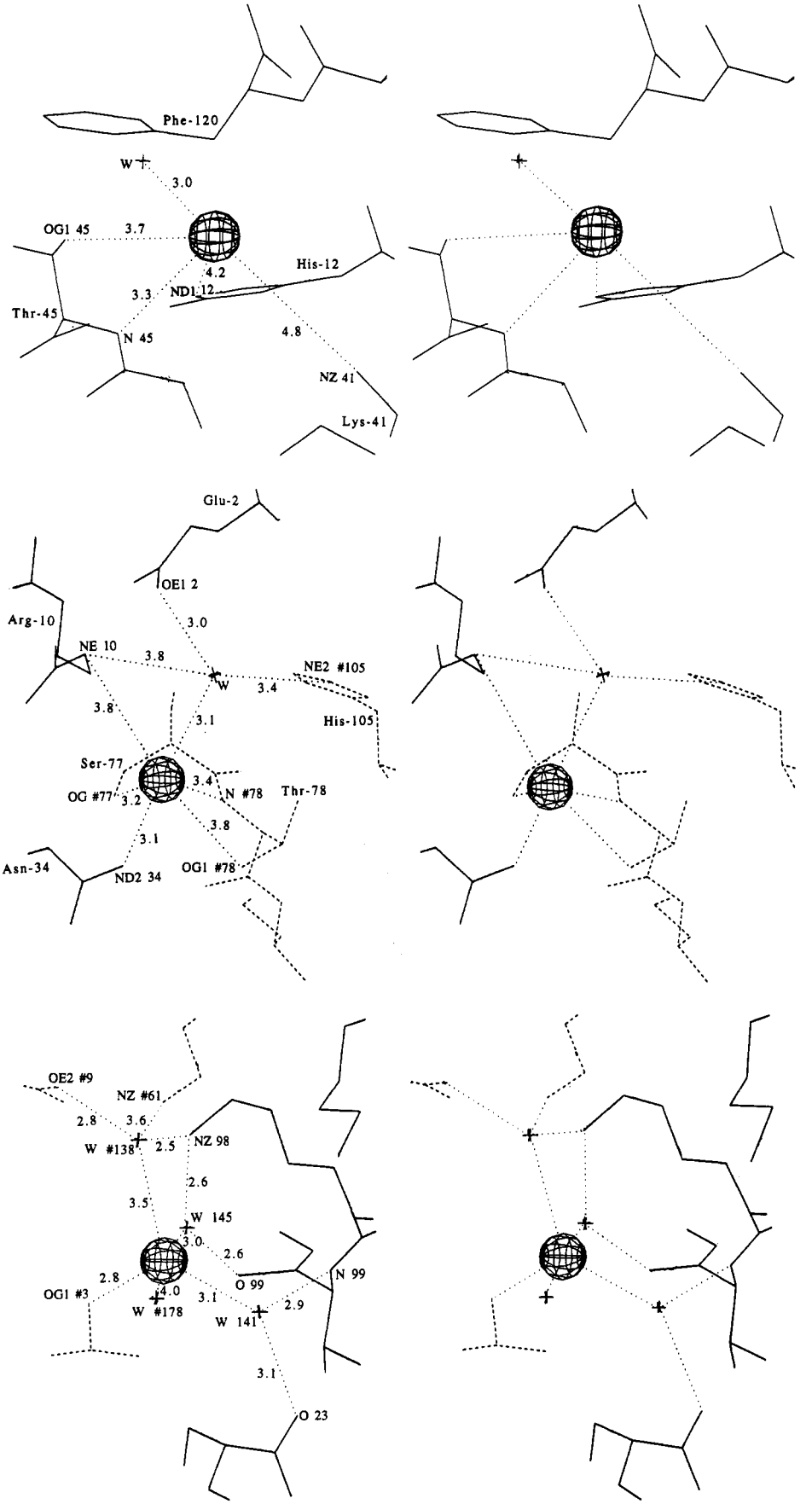

FIGURE 6: Chloride sites in model II (3 M NaCl): (a, top) chloride 1 is next to His-12 in the active site (polar atoms within 4 Å belong to Thr-45 and a water molecule); (b, middle) chloride 2 is within 4 Å of polar groups belonging to Arg-10 and Asn-34 of one RNase molecule, to Ser-77 and Thr-78 of another (- - -), and to a water molecule; (c, bottom) chloride 3 is bound to W141, W145, W138, and W178, associated with residues 98-99 of one molecule and the hydroxyl of Thr-3 from another molecule (- - -). The nearest positive charge is 4.3 Å away on Lys-98.

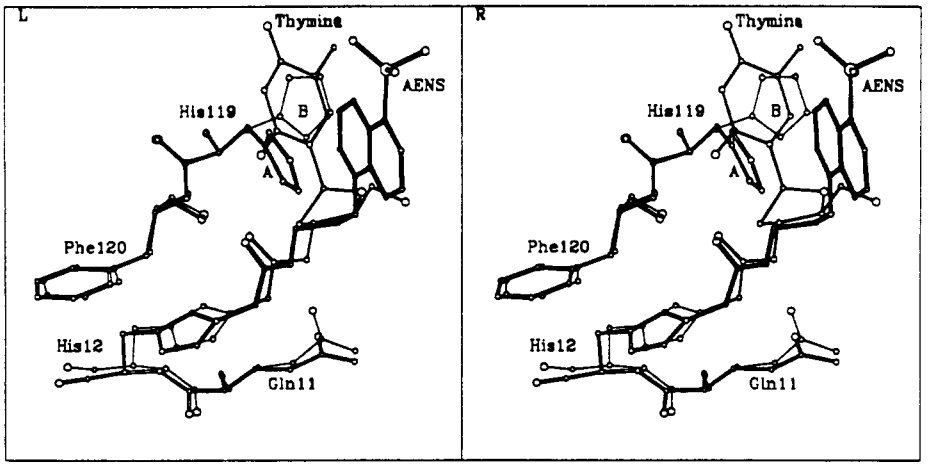

FIGURE 7: Active site of the AENS-RNase and T-His-12-RNase. T-His-12-RNase (Nachman et al., 1990; file 8RSA) is drawn as thin lines superimposed onto model I of AENS-RNase (thick lines). The thymidine substituent is linked to His-12 and stacks on His-119 very much like AENS, but the side chain of His-119 has moved from the A to the B position by rotating about the C^{α}–C^{β} bond.

the whole protein. The anisotropy almost vanishes upon denaturation as the probe rotates more freely. Though tightly bound in the native state, the probe is accessible to acrylamide, which quenches its fluorescence with about the same rate constant as in the unfolded state. Moreover, the fluorescence intensity in the native state shows an unusually strong temperature dependence, which was attributed to conformational fluctuations on the nanosecond time scale (Jullien et al., 1986).

The crystal structures of AENS-RNase described here confirm that 1,5-IAENS preferentially reacts with His-12. They also show that the naphthyl ring stacks on the imidazole group of the other catalytic histidine, His-119. The stacked ring is still largely accessible to solvent and to molecules like acrylamide, yet it has one face in contact with protein atoms which cannot reorient freely as solvent molecules do. We attribute to this contact the reduction of the Stokes shift and the blue shift of the emission maximum from 500 nm down to 480 nm. A blue shift of the emission spectrum is commonly taken to indicate that the probe has moved to a hydrophobic environment. The protein environment of the probe here is the RNase active site, which includes many polar and charged groups. These contribute 50% of the protein surface area involved in contacts with the fluorophore (200 Å^2), while they form 43% of the total accessible surface of RNase A. Thus, the usual interpretation of the shift is apparently incorrect in this case, and most likely in many others as well. Partial removal of a fluorescent probe, whether extrinsic as in this case or intrinsic (tryptophan) from contact with water, is a sufficient explanation for the blue shift.

If the stacking interaction is assumed to be stable on a nanosecond time scale, the ring is unable to flip during the lifetime of the excited state. The high anisotropy of the fluorescence can be explained without implying complete immobilization of the probe. The poor electron density and high *B* factors of the naphthyl and sulfonate groups suggest that the fluorophore undergoes fast in-plane movements while remaining stacked on His-119. Alternatively, it may have multiple positions with occupancies much lower than the stacked one. In the T-His-12-RNase structure, a nucleotide analog is covalently attached to His-12 while the thymidine base stacks on the His-119 imidazole just as the naphthyl does, although the imidazole is in a different position. In that crystal structure also, the stacked base has poor density and high *B* factors (Nachman et al., 1990). The linker group makes the same interaction as ours with the NH of Phe-120, but the ribose and the base do not superimpose with the AENS molecule. The limited possible rotations of the probes may favor packing onto His-119 in the B position for the thymine, and in the A position for the naphthyl group (Figure 7).

The study of RNase A precrystallization by Crosio and Jullien (1992) made use of the fluorescence anisotropy of the AENS reporter group. In high salt or in ethanol solutions where the protein was still soluble, the anisotropy was strongly dependent on protein concentration, indicative of increasing interactions between RNase molecules. Most of the protein was unlabeled, so that interactions between fluorophores on different molecules could be neglected. The present results confirm that AENS-RNase has essentially the same structure as native RNase A, that it yields the same crystal packing as observed in other RNase structures, and that the fluorophore is not involved in crystal contacts. Thus, the crystallographic study validates the use of the fluorescent derivative in the work of Crosio and Jullien (1992).

The finding that NaCl can replace CsCl as a precipitant while crystallizing RNase A (Crosio & Jullien, 1992) led us to collect two sets of diffraction data, one in high ammonium sulfate and the other in high NaCl, and to do parallel refinements against both. The two models are essentially identical, with a few differences in the solvent region. No sulfate ion was detected in model I, and only three chloride ions in model II. Bound anions do not neutralize the total charge of RNase A (+8, assuming all four histidines are protonated at pH 5.1). Other anions, chloride or sulfate, must be present, but they are not ordered.

The small number of bound anions fits with the data of Saroff and Carroll (1962) on chloride binding. On the other hand, a calculation of the electric potential at the protein surface located two potential chloride binding sites on RNase A at pH 6 and at least five at pH 4 (Matthews & Richard, 1982). The pH 6 sites are in between His-12 and His-119; one of them may be chloride 1. Another site was predicted near Arg-10, like chloride 2. However, chlorides 2 and 3 are located at interfaces between RNase molecules and, presumably, they are crystallization artifacts. Each of the three chloride ions is near one of the many cationic groups of the protein, but no clustering of positive charges is observed around them. Very few chloride binding sites have been described in protein crystal structures. In the deoxyhemoglobin Rothschild mutant (37βTrp > Arg), a chloride ion is at the $\alpha\beta$ subunit interface, bound to the mutated Arg37β (Kavanaugh et al. (1992). In phage T4 lysozyme crystals, a chloride ion

is at a molecular interface and binds to main chain amides. The site is lost in the N144D mutant where water molecules replace the ion (Nicholson et al., 1988).

In our model I, chlorides 2 and 3 are replaced by water rather than by sulfate ions, with very little change in the local structure. Therefore, the anions at molecular interfaces are not essential for protein or crystal stability, although they could still be involved in nucleation or growth.

ACKNOWLEDGMENT

We thank Dr. P. Martin (Detroit, MI) for sending us coordinates prior to deposition and the technical staff of LURE (Orsay, France) for help during data collection.

REFERENCES

Bernstein, F. C., Koetzle, T. F., Williams, G. J. B., Meyer, E. F., Brice, M. D., Rodgers, G. R., Kennard, O., Shimanouchi, T., & Tasumi, M. (1977) *J. Mol. Biol. 112*, 535–543.
Borkakoti, N. (1983) *Eur. J. Biochem. 132*, 89–94.
Borkakoti, N., Moss, D. S., & Palmer, R. A. (1982) *Acta Crystallogr., Sect. B 38*, 2210–2217.
Campbell, R. L., & Petsko, G. A. (1987) *Biochemistry 26*, 8579–8584.
Chothia, C., & Lesk, A. M. (1986) *EMBO J. 5*, 823–826.
Crosio, M.-P., & Jullien, M. (1992) *J. Cryst. Growth 122*, 66–70.
Crosio, M.-P., Janin, J., & Jullien, M. (1992) *J. Mol. Biol. 228*, 243–251.
DeMel, V. S. J., Martin, P. D., Doscher, M. S., & Edwards, B. F. P. (1992) *J. Biol. Chem. 267*, 247–256.
Doscher, M. S., Martin, P. D., & Edwards, B. F. P. (1983) *J. Mol. Biol. 166*, 685–687.
Finzel, B. C. (1987) *J. Appl. Crystallogr. 20*, 53–55.
Heinrikson, R. L., Stein, W. H., Crestfield, A. M., & Moore, S. (1965) *J. Biol. Chem. 240*, 2921–2934.
Hendrickson, W. A. (1985) *Methods Enzymol. 115*, 252–270.
Howards, A. J., Gilliland, G. L., Finzel, B. C., Poulos, T. L., Ohlendorf, D. H., & Salemne, F. R. (1987) *J. Appl. Crystallogr. 20*, 383–387.
Hudson, E. N., & Weber, G. (1973) *Biochemistry 12*, 4154–4161.
Jones, T. A. (1978) *J. Appl. Crystallogr. 11*, 268–272.
Jullien, M., & Garel, J.-R. (1981) *Biochemistry 20*, 7021–7026.
Jullien, M., & Crosio, M.-P. (1991) *J. Cryst. Growth 110*, 182–187.
Jullien, M., Garel, J.-R., Merola, F., & Brochon, J.-C. (1986) *Eur. Biophys. J. 13*, 131–137.
Kavanaugh, J. S., Rogers, P. H., Case, D. A., & Arnone, A. (1992) *Biochemistry 31*, 4111–4121.
Martin, P. D., Doscher, M. S., & Edwards, B. F. P. (1987) *J. Biol. Chem. 262*, 15930–15938.
Matthews, J. B., & Richard, F. M. (1982) *Biochemistry 21*, 4989–4999.
Nachman, J., Miller, M., Gilliland, G. L., Carty, R., Pincus, M., & Wlodawer, A. (1990) *Biochemistry 29*, 928–937.
Nicholson, H., Becktel, W. J., & Matthews, B. W. (1988) *Nature 336*, 651–656.
Saroff, H. A., & Carroll, W. R. (1962) *J. Biol. Chem. 237*, 3384–3387.
Sheriff, S. (1987) *J. Appl. Crystallogr. 20*, 55–57.
Stryer, L. (1968) *Science 162*, 526–533.
Sussmann, J. L., Holbrook, S. R., Church, G. M., & Kim, S. H. (1977) *Acta Crystallogr., Sect. A 33*, 800–804.
Svensson, L. A., Dill, J., Sjölin, L., Wlodawer, A., Toner, M., Bacon, D., Monet, J., Vecrapandia, B., & Gilliland, G. L. (1991) *J. Cryst. Growth 110*, 119–130.
Wlodawer, A. (1985) in *Biological Macromolecules and Assemblies*, Vol. II, Nucleic Acids and Interactive Proteins (Jurnak, F., & McPherson, A., Eds.) pp 395–439, Wiley, New York.
Wlodawer, A., Bott, R., & Sjölin, L. (1982) *J. Biol. Chem. 257*, 1325–1332.
Wlodawer, A., Svensson, L. A., Sjolin, L., & Gilliland, G. L. (1988) *Biochemistry 27*, 2705–2717.